Influence of elastic properties on the strain induced by ion irradiation in crystalline materials

A. Debelle, Alexandre Boulle, F. Rakotovao, J. Moeyaert, C. Bachelet, F. Garrido, L. Thome

Influence of elastic properties on the strain induced by ion irradiation in crystalline materials

A. Debelle[a*], A. Boulle[b], F. Rakotovao[a], J. Moeyaert[a], C. Bachelet[a], F. Garrido[a], L. Thomé[a]

a. Centre de Spectrométrie Nucléaire et de Spectrométrie de Masse (CSNSM), Univ. Paris-Sud, CNRS-IN2P3, 91405 Orsay Cedex, France
b. Science des Procédés Céramiques et de Traitements de Surface (SPCTS), CNRS UMR 6638, Centre Européen de la Céramique, 12 rue Atlantis, 87068 Limoges, France

Abstract

Cubic zirconia, an elastically anisotropic material, has been irradiated with 300 keV Cs^+ ions and the irradiation-induced elastic strain has been measured using X-ray diffraction (XRD). In order to highlight the influence of the elastic properties on the strain level, two different cases have been investigated: (i) {100} *vs.* {111}-oriented zirconia single crystals and (ii) {100} zirconia *vs.* {100} strontium titanate. In the former case, raw experimental results show that {100} planes deform less than {111} planes. However, with a modelling that takes into account the effect of the elastic properties, it is demonstrated that the strain due to irradiation defects only is the same for both orientations (with a maximum value of ~0.8%). Combined use of this modelling and of a dedicated computer program for fitting XRD data allowed determining both defect concentration (~1%) and relaxation volume (~0.5 atomic volume). In the latter case, it is shown that elastic properties affect the measured strain in irradiated zirconia and strontium titanate. However, a difference between the two materials remains even taking into account this effect, confirming that different compounds of a same class of materials (namely ceramic oxides) can exhibit a different response to ion irradiation.

*Corresponding author, e-mail: aurelien.debelle@u-psud.fr
PACS: 61.80.-x; 62.20.D-; 61.05.cp;

1. INTRODUCTION

Ion beams are currently used in many fields of materials science and engineering. Two examples are particularly illustrative of their high usefulness: (i) ion implantation is a technique that has become an attractive way of controlled local dopant introduction in many materials, especially in semiconductors [1]; (ii) ion irradiation is used as a tool to simulate, in a controlled way, various radiation environments such as those encountered in, e.g., space [2] or nuclear power plants [3]. Consequently, a very large number of studies devoted to the behaviour of materials subjected to ion irradiation have been carried out during the last five decades (for a recent review see [4]). One of the main objectives of these works lies in the understanding of damage formation during this severe out-of-equilibrium process. For this purpose, many experimental characterization techniques were implemented, the most common ones being probably Raman spectroscopy, Rutherford Backscattering Spectrometry in the channelling mode (RBS/C), transmission electron microscopy (TEM) and X-ray diffraction (XRD). Regarding this latter technique, an important parameter that can be monitored in crystalline materials is the irradiation-induced elastic strain generally associated to defect formation. The growing number of recent publications dealing with the correlation between irradiation damage and strain level demonstrates that this kind of study currently witnesses a renewed interest [see *e.g.* 5-11].

In the two above-mentioned fields (*i.e.* doping of semiconductors or simulation of radiation environments), investigations usually deal with bulk crystals. However, except when very energetic ions (typically with a few MeV/nucleon) are used, only a shallow layer (namely from a few tens of nanometers to a few microns) at the specimen surface is altered by the irradiation process. It becomes thus relevant to consider the

material not as a bulk but rather as a thin (irradiated) layer on a substrate, the latter being the undamaged part of the crystal. In this case, it has been demonstrated that the mechanical response of the sample can be described using a two-step model [7,12]. In the first step, irradiation defects induce in the thin layer submitted to ion irradiation a local lattice volume change characterized by an isotropic strain $\varepsilon_{(hkl)}^{def}$; in the second step, since mechanical constraints of the underlying thick substrate prevent any lateral macroscopic dimensional change, the thin irradiated layer is subjected to an in-plane biaxial compressive stress $\sigma_{//}$ which totally cancels the in-plane components of $\varepsilon_{(hkl)}^{def}$. The development of this stress results in an additional tensile-strain contribution $\varepsilon_{(hkl)}^{SR}$ in the direction normal to the surface (out-of-plane strain), due to the substrate reaction (SR) by Poisson effect. This contribution is proportional to $\varepsilon_{(hkl)}^{def}$ and depends on the elastic constants of the material. Thus, the substrate reaction may vary (i) for two different materials with different elastic constants and (ii) with the crystallographic orientation for an elastically anisotropic crystal. Therefore, in order to compare the response of different materials under irradiation, it is mandatory to account for this purely mechanical contribution, since it is the total strain that is experimentally measured. A model was developed in the early 1990's by Rao *et al.* [12] to separate both strain contributions in ion-irradiated materials. This model has been recently renewed by the authors of the present paper, using a modelling initially developed for sputtered thin films [13], in the framework of materials for nuclear energy applications and in particular in {100}-oriented urania [14] and yttria-stabilized cubic zirconia (YSZ) [7,15] crystals. However, a detailed study that demonstrates the possible effects of the elastic properties on the irradiation-induced strain in different situations has never

been presented. A few works where XRD measurements have been carried out dealt with this topic. For instance, the influence of the crystalline orientation has been tested by Pesek [16] in Ge-implanted {001}- and {111}-oriented silicon wafers, and by Sousbie et al. [17] in H-implanted silicon crystals oriented along <001>, <100> and <111> directions. In both cases, the strain level has been found to depend on the crystalline orientation, but, although the particular mechanical situation has been precisely described (namely a thin irradiated layer attached to a thick substrate), the strain due to irradiation defects only has not been calculated.

In this paper, the irradiation-induced strain has been monitored in two different cases. In the first situation, cubic zirconia has been chosen as a test-case for elastically anisotropic materials and both {100}- and {111}-oriented crystals have been subjected to low-energy ion irradiation. Relationships that allow separating defect-related and purely-mechanical-related contributions are provided for these two crystalline orientations in any cubic crystals. In addition, using this modelling and data obtained from the fitting of the XRD curves, information on defect concentration and relaxation volume are provided. In the second case, a comparison between zirconia and strontium titanate (STO) is presented.

2. EXPERIMENTAL

The samples used in this study are {100} and {111}-oriented (cubic) YSZ and {100}-oriented STO single crystals, whose bulk pristine lattice parameter are 0.5145 nm and 0.3905 nm, respectively. Both YSZ and STO crystals are elastically anisotropic,

with an anisotropy factor defined as $C_{an} = C_{44} - 1/2(C_{11} - C_{12})$; values of elastic stiffnesses C_{ij} (from Refs. [18-19]) and of C_{an} are given in Table I.

Samples have been irradiated, using the IRMA low-energy accelerator of the CSNSM (Orsay-France), at room temperature with 300 keV Cs^+ ions (for which the nuclear energy loss is predominant) at fluences (i.e. number of particles per unit surface) ranging from $2x10^{13}$ cm^{-2} to $5x10^{15}$ cm^{-2}. Irradiations were performed 7° off the normal of the crystal surface to avoid channelling phenomena, and a beam raster system was used to ensure uniform ion irradiation; besides, in order to minimize target heating, the ion current during irradiation did not exceed 0.5 $\mu A.cm^{-2}$. The mean projected range (*i.e.* the maximum of the Gaussian-type distribution) of Cs^+ particles has been estimated, based on dedicated SRIM calculations [20], to be $R_P \sim 67$ nm with a range straggling $\Delta R_P \sim 25$ nm. It is finally important to mention that for each irradiation fluence, (i) {100} and {111}-oriented YSZ crystals, or (ii) {100}-oriented YSZ and STO crystals, have been simultaneously irradiated in order to avoid any discrepancy in the fluence that may lead to differences in the measured strain.

The strain has been determined from XRD measurements using two different diffractometers in order to verify the reproducibility of the obtained strain values. The two diffractometers are extensively described in [21] and [22]. It is worth mentioning here that both equipments deliver a monochromatic ($Cu_{K_{\alpha 1}}$ radiation, λ=0.15406 nm) incident X-ray beam with a very weak divergence (~18 arcsec, *i.e.* 0.005°, and ~12 arcsec, *i.e.* 0.003°, respectively for [21] and [22]), allowing high-resolution measurements of diffraction lines in single-crystals. Symmetric θ-2θ scans were recorded in the vicinity of the (400) Bragg reflection of {100} YSZ samples ($2\theta \sim 73.575°$) and around the (200) Bragg reflection of {100} STO crystals

(2θ ~ 46.47°); the (222) Bragg reflection was recorded for {111} YSZ samples (2θ ~ 62.48°). The formalism used in this paper is the one presented in Ref. [7], and is based on the work of Dederichs with regard to the treatment of diffuse X-ray scattering [23]. Since only symmetric reflections were analyzed, only the following parameters are necessary in the present study: (i) $K = 2sin\theta/\lambda$ is the scattering vector; (ii) $H_{(hkl)}$ refers to the reciprocal lattice vector for the symmetric (hkl) reflection; (iii) q is defined as $K\text{-}H_{(hkl)}$ and represents the deviation from the reciprocal lattice vector (sometimes called reduced scattering vector); (iv) $(-q/H_{(hkl)})$ is equal to the elastic strain in the direction normal to the surface of irradiated samples, ε. It is worth noting that in the present case, all these vectors have for sole component the normal (out-of-plane) component.

Complementary RBS/C experiments were also carried out at in random and channelling geometries by using a $^4He^{2+}$ beam at 3.07 MeV. The energy resolution of the experimental setup was about 15 keV. The depth distribution of the disorder fraction f_D, which represents the fraction of atoms that are randomly displaced from their equilibrium position, was extracted from the analysis of RBS/C spectra with Monte-Carlo simulations performed by using the McChasy computer code [24].

3. RESULTS AND DISCUSSION

3.1. Strain and stress levels

Figure 1 displays symmetric θ-2θ scans recorded for virgin and irradiated {100} (Fig. 1a) and {111} (Fig. 1b) YSZ single crystals. It is immediately observed that the shape of XRD patterns is similar for both orientations. All spectra exhibit an intense narrow peak on the high-angle side which corresponds to the unirradiated part of

samples (*i.e.* the substrate); this finding was expected since the depth probed by X-rays in this configuration reaches ~4 μm (1/e attenuation-length criterion), which is much greater than the irradiated thickness (~150 nm). In the following, this peak will be considered as an internal strain gauge that allows quantifying the irradiation-induced elastic strain. An additional signal at low 2θ angle is recorded for irradiated crystals. This observation indicates that a tensile elastic strain developed in the irradiated layers. Furthermore, except at the highest fluence ($5x10^{15}$ cm^{-2}), this signal exhibits a fringe pattern that indicates the presence of a dilatation gradient along the direction normal to the sample surface [see *e.g.* 5-9,12]. It is possible to retrieve the corresponding strain depth profile but this requires achieving a complete fitting of the XRD curves using the dynamical theory of X-ray diffraction [25]. Simulations of selected experimental XRD data are presented below. However, the maximum total strain exhibited by irradiated layers can be, in the present case, easily obtained directly from the position of the last fringe on the low-angle side of the diffraction curves. It is thus observed that the irradiation-induced (elastic) strain increases with the fluence. This result holds for both crystallographic orientations. At the highest fluence, Bragg diffraction (arising from the irradiated layer) is superseded by diffuse scattering. It has been demonstrated that this dramatic change can be explained considering that the irradiated layer does not anymore respond elastically to the radiation damage, the relaxation of the strained layer being driven by the development of plastic strain (*i.e.* formation of extended defects) [10,14,26]. Consequently, at this fluence, the elastic strain is assumed to be almost completely relaxed, and the remaining strain level is roughly deduced from the barycentre of the broad diffuse peak.

The variation with the irradiation fluence of the (maximum) total elastic strain $\varepsilon_{(hkl)}^{total}$ experienced by irradiated layers is displayed in Fig. 2 (open symbols). For both crystallographic orientations, the (maximum) total strain is found to increase with irradiation fluence until it is drastically relieved (this relaxation phenomenon has already been shown in an identical situation in [15]). Nevertheless, the values measured for both orientations appear to be very different. Actually, at each fluence, the strain level experienced by {111} layers is much larger than that exhibited by {100} ones. For instance, just before the onset of relaxation, the total strain reaches ~1.7% in the {111} crystal while it only amounts to ~1.25% in the {100} layer. This finding would tend to indicate that both crystalline orientations respond differently to ion irradiation. But it is worth reminding that this total strain is the sum of two contributions: the strain due to irradiation defects, $\varepsilon_{(hkl)}^{def}$ and the strain that arises from the substrate reaction, $\varepsilon_{(hkl)}^{SR}$. Therefore, in order to properly compare the results obtained for both crystalline orientations, it is mandatory to account for the substrate reaction. Using the model presented in the Introduction and extensively described in [7] and [12], the two strain components are linked through the following relationship:

$$\varepsilon_{(hkl)}^{total} = \varepsilon_{(hkl)}^{def}(1+\alpha_{(hkl)}^{SR}) \quad (1)$$

where $\alpha_{(hkl)}^{SR}$ is a parameter that describes the substrate reaction and that only depends on the elastic constants of the material. Using the anisotropic elasticity calculations presented in [27], $\alpha_{(hkl)}^{SR}$ is defined as:

$$\alpha_{(hkl)}^{SR} = \left(\frac{2C_{12} - C_{an}\Omega_{(hkl)}}{C_{11} + C_{an}\Omega_{(hkl)}} \right) \quad (2)$$

where $\Omega_{(hkl)}$ is a geometric factor (equal to 0 for (100) planes and to 4/3 for (111) planes) that relies on direction cosines of the sample coordinate system with respect to the cubic coordinate system. $\alpha^{SR}_{(hkl)}$ values are reported in Table I. It can be noted that the contribution of the substrate reaction is nearly 2.5 times larger for the {111} orientation than for the {100} orientation. Using Eqs. (1) and (2), it becomes possible to separate the strain due to the formation of irradiation defects from the strain due to the substrate reaction (thus due to purely elastic effects). The variation of the former, $\varepsilon^{def}_{(hkl)}$, with the irradiation fluence is displayed in Fig.2 (full symbols) for both crystallographic orientations. It is striking to observe that at each ion fluence the strain level due to irradiation defects only is the same for both orientations, whereas it seemed that, without taking care of the substrate reaction, one orientation was more sensitive to ion irradiation than the other one. But the experimentally measured total strain is found to be larger for {111} than for {100} planes only because of the elastic anisotropy of zirconia. Indeed, the anisotropy factor of this material is negative, meaning that the {111} planes are more compliant than the {100} ones, allowing a larger strain to develop for a same mechanical solicitation. Similarly, irradiated layers experience an in-plane compressive stress that depends on the orientation. Using the modelling above-described, it is possible to derive the corresponding stress values [7,12]. Maximum stress levels (before the onset of relaxation) of -4.1 GPa and -2.3 GPa are found for <100> and <111> orientations, respectively. Such large values confirm that low dimensional materials can sustain high stress levels.

The fact that both crystallographic directions exhibit a same strain level if the sole presence of irradiation defects is considered gives rise to two important comments. First, irradiation defects must be, statistically, isotropically distributed in the crystalline

lattice. This statement is consistent with the fact that defect production generated in collision cascades that develop during ion irradiation in the nuclear energy-loss regime is a stochastic process. Second, at a given ion fluence, irradiation seems to produce equal defect concentration whatever the crystallographic orientation, assuming that same defects are produced in both directions (this statement is confirmed in sect. 3.2.). RBS/C data and the corresponding depth profiles presented in Fig.3 for crystals irradiated to two fluences in both directions support this assertion. The disorder level (f_D) measured just before the onset of relaxation, i.e. at $7.5x10^{14}$ cm^{-2}, is found to be weak, which is an indication of the presence of small defects (or defect clusters), and very similar for both directions. This result is in agreement with a study conducted by Wendler et al. [28] that dealt with radiation damage along different crystallographic orientations in MgO and where it was demonstrated that the disorder level does not depend on the direction at low irradiation level. This finding supports the assumption that an equal defect concentration is present in the two different types of crystals. After strain relaxation (at $5x10^{15}$ cm^{-2} for instance), the disorder level strongly increases, which is an indication of the formation of a new type of defects, presumably dislocation loops. Both decrease of elastic strain and increase of disorder fraction seem to occur at the same irradiation fluence (in complete agreement with previous studies [14,15,29]), and thus, in the present case, at the same defect concentration. This result suggests that the total strain does not trigger the relaxation, but rather that the defect density does. After relaxation, f_D is still the same for both directions, in agreement with a study carried out by Usov. et al. [30] that showed using RBS/C that the damage depth distribution is very similar in both <100> and <111> directions in YSZ, even at high disorder level (f_D~0.7). Although out of the scope of the paper, it is worth mentioning

that in both MgO [28] and YSZ [30] crystals, at high irradiation level, a lower disorder fraction has been observed along the <110> direction than along the two other main directions: the anisotropy of the dynamic annealing rate has been invoked to explain such a discrepancy.

3.2. Strain and damage profiles

XRD patterns corresponding to YSZ crystals exhibiting the highest elastic-strain level have been fitted following the procedure described in details elsewhere [22]. These simulations are presented in Fig.4a for both orientations. From these simulations, the strain depth profiles have been retrieved (Fig. 4b). These strain distributions exhibit a "bell curve" shape, identical to that previously obtained for similar {100}-oriented Cs-irradiated crystals [15,25]. It is interesting to note that the shape and the spatial extent of these profiles are totally comparable for both crystallographic orientations.

From the XRD simulations, it is also possible to have access to the damage profiles (Fig.4b), which are also found to be similar to those previously obtained for analogous Cs-irradiated crystals [25]. These damage profiles represent the depth distributions of the so-called static Debye-Waller factor, $\exp(-L_H)$ [23], a parameter that is responsible for a lowering of the scattered amplitude due to the presence of atoms displaced from their regular crystallographic site. The static Debye-Waller factor is considered as a characteristic parameter of the clustering degree of point defects. In the framework of the superposition model, in which point defects are clustered together such that their displacement fields simply superimpose on each other, and assuming a large defect density (and/or a high order reflection), L_H is defined as [23]:

$$L_H = \frac{2\sqrt{2\pi}}{15} H_{hkl}^{3/2} \frac{(\Delta V_{cl})^{3/2}}{V_\Omega} c_{cl} \qquad (3)$$

where ΔV_{cl} refers to the so-called relaxation volume of a cluster (expressed here in atomic volume unit, $V_\Omega \sim 1.625 \times 10^{-3}$ nm^3 for YSZ) and c_{cl} represents the cluster concentration. This volume change is linked to the strain through the following relation:

$$3\varepsilon^{def} = c_{cl} \frac{\Delta V_{cl}}{V_\Omega} \quad (4)$$

It is worth emphasizing that the strain component in Eq.(4) is not the total strain, but the strain that is due to defects only, and this latter is precisely obtained via the modelling presented in this paper. Using Eqs. (3) and (4) for the highest fluence used here (which corresponds to the highest elastic strain level for which assumptions that allowed deriving Eq.(3) should hold), one obtains the following values (at the maximum of the strain and damage distributions): $\Delta V_{cl}^{(100)} \sim 0.7\Omega$, $\Delta V_{cl}^{(111)} \sim 0.45\Omega$, $c_{cl}^{(100)} \sim 1.55\%$, $c_{cl}^{(111)} \sim 0.9\%$. Considering the roughness of Eq. (3), it is reasonable to conclude that values are similar for both orientations, confirming again that the irradiation-induced damage does not depend on the crystallographic orientation. It should also be pointed out that the values obtained for the relaxation volumes are very small, especially comparing those found in YSZ crystals irradiated with 4 MeV Au^+ ions at 800°C where V_{rel} is ~4Ω at equivalent ion fluence (this work is underway). This small value indicates, as also suggested by the low disorder level obtained by RBS/C, that defect clustering is not significant in the present conditions; it could also be the result of positive and negative relaxation volumes associated to different types of defects.

3.3. Beyond mechanical effects

The model has also been applied to compare the response of YSZ and STO crystals submitted to ion irradiation. Samples have the same crystallographic orientation

(namely {100}), but different elastic properties (see Table I). In particular, the substrate reaction factor is equal to ~0.49 for YSZ while it is ~0.68 for STO. Both sets of samples were simultaneously irradiated at two fluences, $2x10^{13}$ cm^{-2} and $4x10^{13}$ cm^{-2}. The corresponding XRD patterns (not shown here) exhibit similar features as those previously presented in Fig.1. Thus, both types of crystals developed a tensile strain profile after irradiation. The total strain (open symbols) and the strain due to defects only (full symbols) experienced by the irradiated layers are plotted as a function of the fluence in Fig.5. It is readily observed that the total strain level in irradiated STO is much higher than that in YSZ. After accounting for the purely mechanical contribution, the difference in the strain only due to irradiation defects is reduced, pointing out the relevancy to use the presented modelling. However, a difference remains between the two materials. More precisely, the strain in YSZ is lower than that measured in STO. Furthermore, with a twice higher fluence (from $2x10^{13}$ to $4x10^{13}$ cm^{-2}), the strain barely increased in YSZ while it doubled in STO. Therefore, STO appears to be clearly much more sensitive to irradiation than YSZ. This statement is not surprising and confirms previous studies that showed, using RBS/C measurements, that STO is easily amorphized upon ion irradiation [31-32], whereas YSZ is able to accommodate high damage levels [29-33]. In the particular case of oxides, the differences observed in the behaviour upon low-energy ion irradiation process may be rationalized using different criterions such as the topological disorder, the iono-covalency of the bonds or the recrystallization rates of each oxide. Besides, it has been recently demonstrated that these characteristics trigger the short-range recombination/re-organization rate, thus the (dynamic) annealing rate of point defects created within collision cascades [34], and this rate really seems to be the key factor that pilots the response of oxides to irradiation.

4. CONCLUSION

The influence of the elastic properties on the response, in terms of elastic strain, of crystalline materials under ion irradiation has been tested, using XRD, in two different cases. First, the strain level has been measured as a function of the ion fluence in {100} and {111} cubic zirconia (YSZ) crystals subjected to 300 keV Cs^+ ion irradiation. Results demonstrate that it is mandatory to take into account, *via* the use of the elastic constants, the macroscopic mechanical behaviour of the material subjected to ion irradiation to properly monitor its response. With this appropriate modelling, it is shown that YSZ crystals exhibit the same strain level in the two orientations, and the maximum elastic strain is found to be ~0.8% before the onset of relaxation. Using this modelling and owing to the use of a dedicated XRD-pattern simulation computer-code, defect concentrations and defect relaxation volumes have been evaluated (~1% and ~0.5Ω, respectively). Second, a comparison of the irradiation-induced strain in YSZ and STO has been carried out and it led to the conclusion that, though mandatory, accounting for the elastic properties of the materials is not sufficient to fully explain the difference between the two materials.

The behaviour of point defects upon irradiation seems to be a key point in the final (macroscopic) response of irradiated materials. Since XRD, through the measurement of elastic strain, is a precise probe of point defects, the methodology presented in this paper constitutes a relevant tool to get insight on the behaviour of materials in the first stage of the disordering process that takes place upon ion irradiation. It is noteworthy that this methodology can be applied to a wide range of materials for different applications, including semiconductors submitted to ion implantation for doping or irradiated metals and ceramics for nuclear applications.

Acknowledgements

This work has been partially funded by the GNR NEEDS (formerly MATINEX). Some of the XRD measurements have been performed at the nanocenter CTU-IEF-Minerve (Orsay, France) that is partially funded by the "Conseil Général de l'Essonne".

References

[1] Schulz M., *Appl. Phys.*, **4** (1974) 91.

[2] Davoisne C., Leroux H., Frère M., Gimblot J., Gengembre L., Djouadi Z., Ferreiro V., d'Hendecourt L. and Jones A., *Astronomy & Astrophysics*, **482** (2008) 541.

[3] Thomé L., Jagielski J. and Garrido F., *Europhys. Lett.*, **47** (1999) 203.

[4] Proceedings of the 16th Radiation Effects In Insulators Conference, *Nucl. Instr. Meth. B,* **286** (2012) 1-364.

[5] Turos A., Gaca J., Wojcik M., Nowicki L., Ratajczak R., Groetzschel R., Eichhorn F. and Schell N., *Nucl. Instr. Meth. B,* **219** (2004) 618.

[6] Decoster S. and Vantomme A., *J. of Phys. D: Appl.Phys*., **42** (2009) 165404.

[7] Debelle A. and Declémy A., *Nucl. Instr. Meth. B,* **268** (2010) 1460.

[8] Autier-Laurent S., Plantevin O., Lecoeur Ph., Décamps B., Gentils A., Bachelet C., Kaitasov O. and Baldinozzi G., *Europhys. Lett.,* **92** (2010) 36005.

[9] Lacroix B., Leclerc S., Declémy A., Lorenz K., Alves E. and Ruterana P., *Europhys. Lett.,* **96** (2011) 46002.

[10] Yang T., Huang X., Gao Y., Wang Ch., Zhang Y., Xue J., Yan S. and Wang Y., *J. Nucl. Mater.*, **420** (2012) 430.

[11] Leclerc S., Beaufort M.-F., J.-F. Barbot, Declémy A., *Europhys. Lett.,* **98** (2012) 46001.

[12] Rao S. I. and Houska C. R., *J. Mater. Sci.*, **25** (1990) 2822.

[13] J.-D. Kamminga, Th. H. de Keijser, R. Delhez, E. J. Mittemeijer, *J. Appl. Phys*., **88** (2000) 6332.

[14] Debelle A., Boulle A., Garrido F. and Thomé L., *J. Mater. Sci.,* **46** (2011) 4683.

[15] Debelle A., Declémy A., Vincent L., Garrido F. and Thomé L., *J. Nucl. Mater.*, **396** (2009) 240.

[16] Pesek A., *Appl. Phys. A*, **58** (1994) 141.

[17] Sousbie N., Capello L., Eymery J. and Rieutord F., *J. Appl. Phys.*, **99** (2006) 103509.

[18] Kandil H.M., Greiner J.D. and Smith J.F., *J. Am. Ceram. Soc*., **67** (1984) 341.

[19] Bell R.O. and Rupprecht G., *Phys. Rev*., **129** (1963) 90.

[20] Ziegler J.F., Biersack J.P. and Littmark U., The Stopping and Range of Ions in Solids, Pergamon, New York, 1985. Available at: www.srim.org.

[21] Debelle A., Thomé L., Boulle A., Moll S., Garrido F., Qasim L. and Rosza P., *Nucl. Instr. Meth. B*, **277** (2012) 14.

[22] Boulle A., Masson O., Guinebretière R., Lecomte A. and Dauger A., *J. Appl. Cryst*., **35** (2002) 606.

[23] Dederichs P.H., *J. Phys. F: Metal. Phys.*, **3** (1973) 471.

[24] Nowicki L, Turos A, Ratajczak R, Stonert A and Garrido F *Nuclear Instruments and Methods in Physics Research Section B: Beam Interactions with Materials and Atoms*, **240** (2005) 277.

[25] Boulle A. and Debelle A., *J. Appl. Cryst*., **43** (2010) 1046.

[26] Speriosu V.S., Paine B.M., Nicolet M-A. and Glass H.L., *Appl. Phys. Lett*., **40** (1982) 604.

[27] Rao S.I. and Houska C.R., *J. Appl. Phys*., **52** (1981) 6322.

[28] Wendler E., Gärtner K. and Wesch W., *Nuclear Instruments and Methods in Physics Research Section B: Beam Interactions with Materials and Atoms*, **266** (2008) 2872.

[29] Moll S., Thomé L., Sattonnay G., Debelle A., Vincent L., Garrido F. and Jagielski J., *J. Appl. Phys*., **106** (2009) 073509.

[30] Usov I.O., Arendt P.N., Groves J.R., Stan L. and DePaula R.F., *Nucl. Instr. Meth. B*, **240** (2005) 661.

[31] Thevuthasan S., Jiang W., Shutthanandan V. and Weber W.J., *Nucl. Instr. Meth. B*, **206** (2003) 162.

[32] Zhang Y., Wang C. M., Engelhard M. H. and Weber W. J., *J. Appl. Phys*., **100** (2006) 113533.

[33] Sickafus K.E., Matzke Hj., Hartmann Th., Yasuda K., Valdez J.A., Chodak P. III, Nastasi M. and Verall R.A., *J. Nucl. Mater*., **274** (1999) 66.

[34] Chartier A., Van Brutzel L. and Crocombette J.-P., *Nucl. Instr. Meth. B*, **286** (2012) 154.

Table I: Elastic stiffnesses C_{ij} (expressed in GPa) for YSZ and STO crystals, from Refs. [18] and [19] respectively and corresponding anisotropy C_{an} and substrate-reaction $\alpha^{SR}_{(hkl)}$ factors.

	C_{11}	C_{12}	C_{44}	C_{an}	$\alpha^{SR}_{(100)}$ / $\alpha^{SR}_{(111)}$
YSZ	397.6	97.1	58.4	-91.85	0.49 /1.15
STO	317.5	102.5	123.5	16	0.65 / 0.54

Figure captions

Figure 1: θ-2θ scans recorded in the vicinity of symmetric reflections for virgin and irradiated YSZ crystals at increasing Cs^+ ion fluences for (a) {100}-oriented crystals and (b) {111}-oriented crystals. Labels correspond to the ion fluences (expressed in cm^{-2}). Curves are shifted vertically for visualization purposes. Note that the top axis corresponds to the total maximum elastic strain.

Figure 2: Variation as a function of the Cs^+ ion fluence of the maximum of both the total elastic strain $\varepsilon_{hkl}^{total}$ (open symbols) and the strain due to defects ε_{hkl}^{def} (full symbols) determined in irradiated YSZ crystals. Strain levels are presented for both {100} (black circles) and {111} (red stars) planes. Lines are drawn for visualization purposes.

Figure 3: (a) RBS spectra (Zr signal) recorded in random (squares) and axial orientations along the <100> and <111> directions of {100}- and {111}-oriented YSZ crystals, respectively, before (crosses) and after (dots and stars) irradiation with 300 keV Cs^+ ions at the indicated fluences (energy of analyzing $^4He^+$ beam: 3.07 MeV). Lines are fits to data using the McChasy simulation code [24]. (b) Depth distributions of the disorder fraction (f_D) derived from simulations presented in (a).

Figure 4: (a) XRD patterns recorded for {100} and {111} YSZ crystals irradiated at a $7.5x10^{14}$ cm^{-2} fluence (which corresponds to the highest strain level) and corresponding simulations obtained following the procedure described in [25]. (b) Strain and damage depth profiles (see text) obtained from the simulations of the XRD patterns presented in Fig.4(a).

Figure 5: Variation as a function of the Cs^+ ion fluence of the maximum of both the total elastic strain $\varepsilon_{hkl}^{total}$ (open symbols) and the strain due to defects ε_{hkl}^{def} (full symbols) determined in irradiated YSZ (black circles) and STO (orange triangles) crystals. Lines are drawn for visualization purposes.

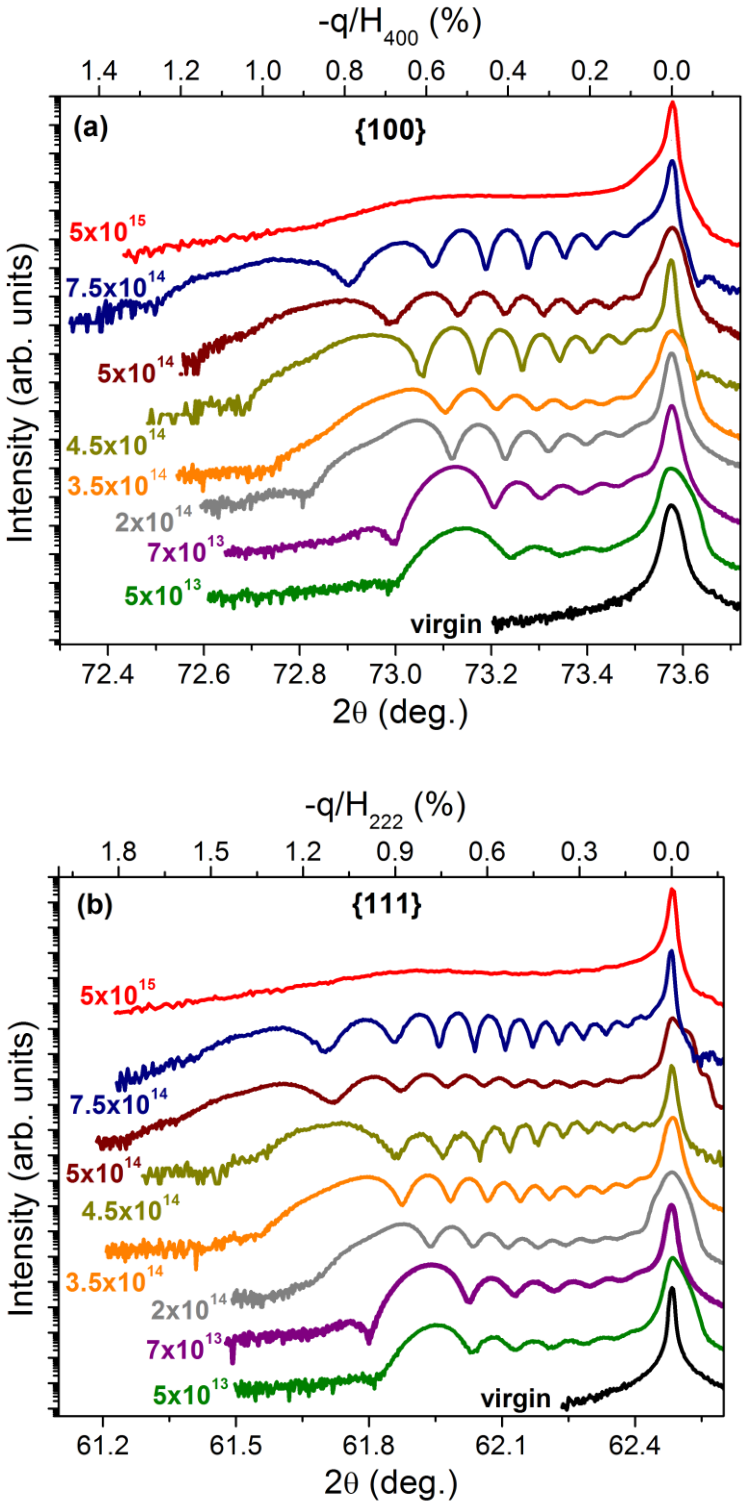
-q/H400 (%)
1.4 1.2 1.0 0.8 0.6 0.4 0.2 0.0
(a)
{100}
5x10^15
7.5x10^14
5x10^14
4.5x10^14
3.5x10^14
2x10^14
7x10^13
5x10^13
virgin
Intensity (arb. units)
72.4 72.6 72.8 73.0 73.2 73.4 73.6
2θ (deg.)
-q/H222 (%)
1.8 1.5 1.2 0.9 0.6 0.3 0.0
(b)
{111}
5x10^15
7.5x10^14
5x10^14
4.5x10^14
3.5x10^14
2x10^14
7x10^13
5x10^13
virgin
Intensity (arb. units)
61.2 61.5 61.8 62.1 62.4
2θ (deg.)

Figure 1

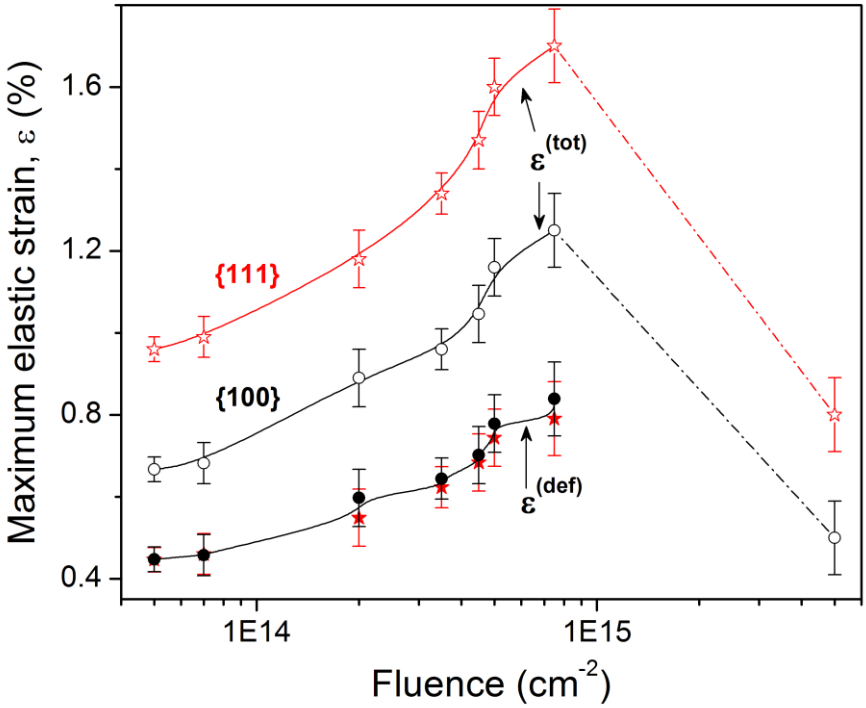
Maximum elastic strain, ε (%)
1.6
1.2
0.8
0.4
{111}
{100}
ε(tot)
ε(def)
1E14
1E15
Fluence (cm-2)

Figure 2

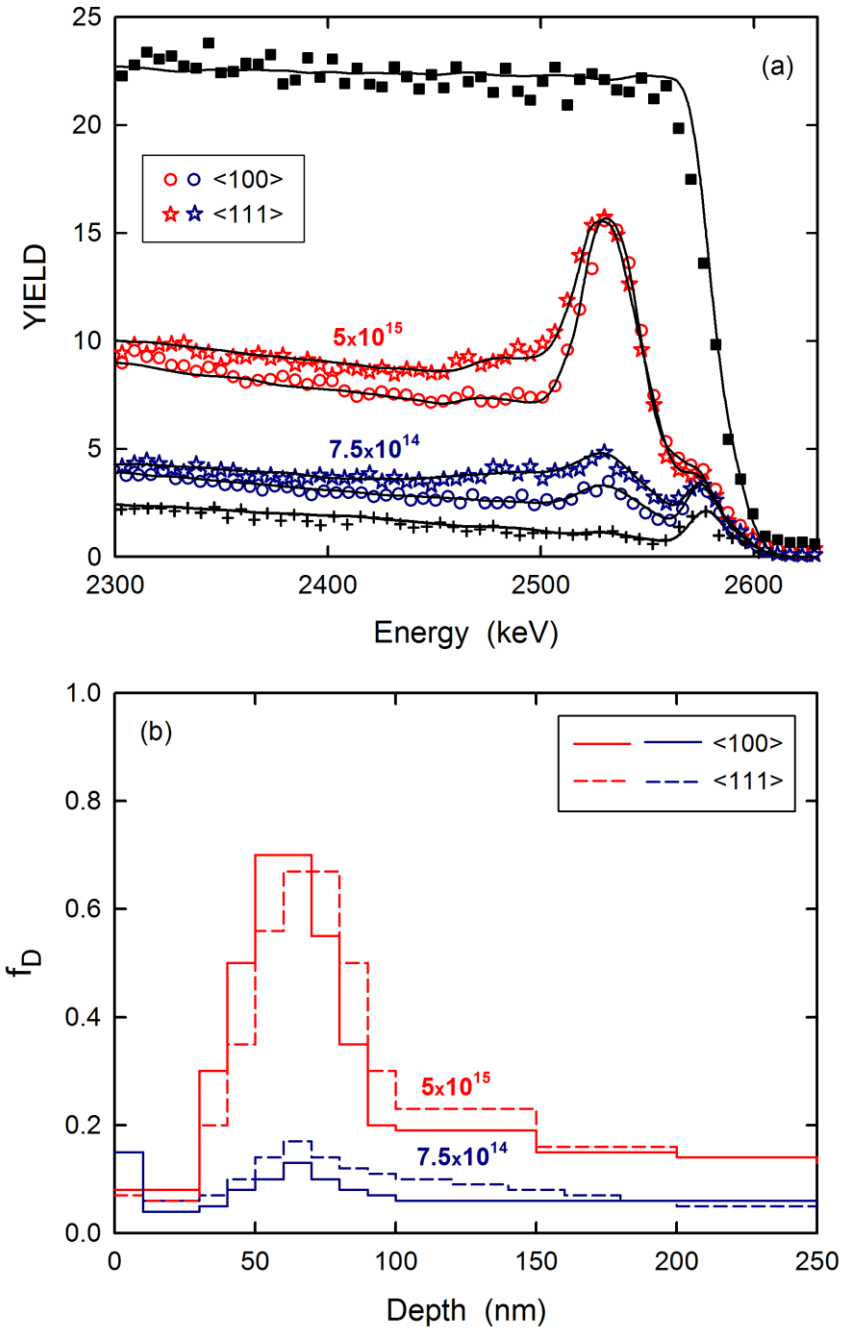
(a)
<100>
<111>
5x10^15
7.5x10^14
YIELD
Energy (keV)
(b)
<100>
<111>
5x10^15
7.5x10^14
f_D
Depth (nm)

Figure 3

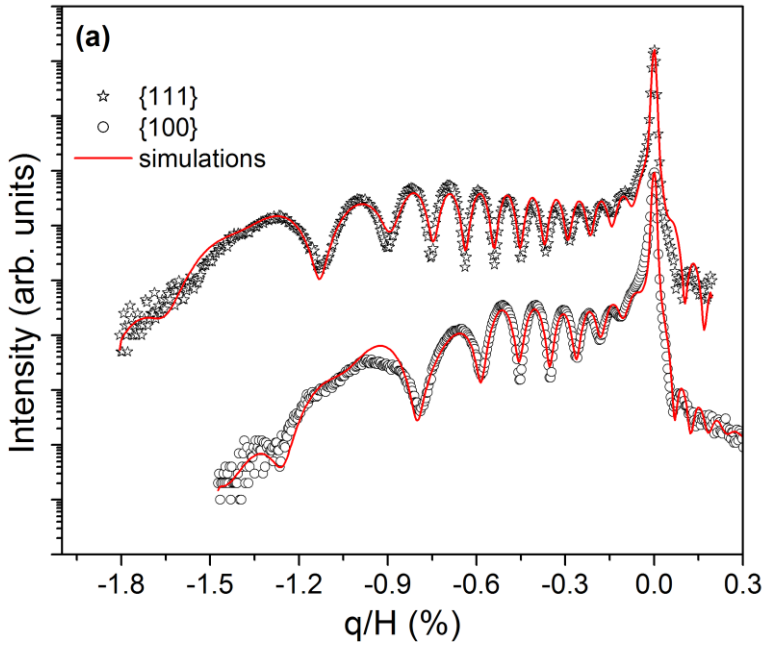
(a)
{111}
{100}
simulations
Intensity (arb. units)
-1.8
-1.5
-1.2
-0.9
-0.6
-0.3
0.0
0.3
q/H (%)

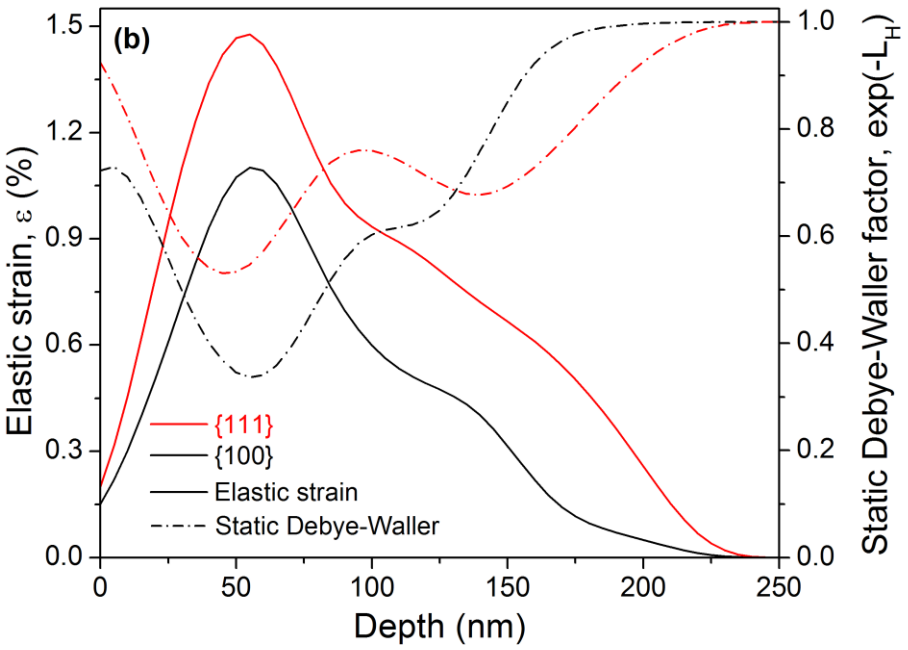
(b)
{111}
{100}
Elastic strain
Static Debye-Waller
Elastic strain, ε (%)
Static Debye-Waller factor, exp(-L_H)
0.0
0.3
0.6
0.9
1.2
1.5
0.0
0.2
0.4
0.6
0.8
1.0
0
50
100
150
200
250
Depth (nm)

Figure 4

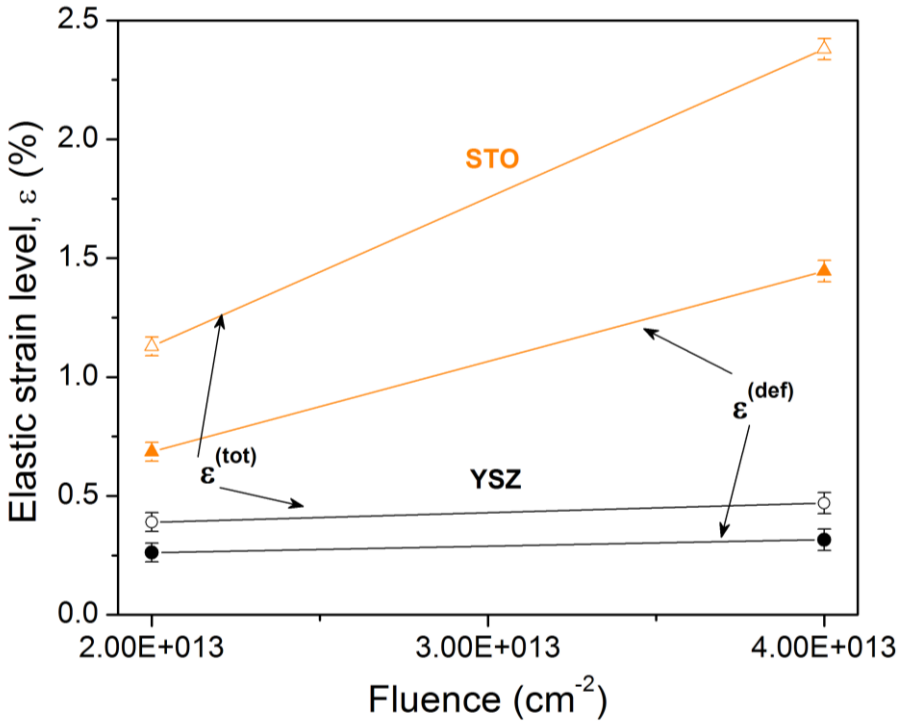
Elastic strain level, ε (%)
2.5
2.0
1.5
1.0
0.5
0.0
STO
YSZ
ε(tot)
ε(def)
2.00E+013
3.00E+013
4.00E+013
Fluence (cm-2)

Figure 5